Electronic Supplementary Material (ESI) for Catalysis Science & Technology.


# Carbon nitride based Schottky junction with Ni-Mo synergistic interaction for high efficient photocatalytic hydrogen production

Lei Ding,[a] Li-Jing Wang,[b] Ru-Yi Liu,[a] Yan-Fei Li,[a] Hai-Zhu Sun*[a]

[a] National & Local United Engineering Laboratory for Power Batteries, College of Chemistry, Northeast Normal University, Changchun 130024, People's Republic of China.

[b] Henan Engineering Center of New Energy Battery Materials, Henan D&A Engineering Center of Advanced Battery Materials, College of Chemistry and Chemical Engineering, Shangqiu Normal University, Shangqiu 476000, People's Republic of China.

* Corresponding authors. E-mail: sunhz335@nenu.edu.cn

## 1. Materials

Analytically pure urea, $Na_2MoO_4 \cdot 2H_2O$, $Ni(NO_3)_2 \cdot 6H_2O$ and $NaH_2PO_2 \cdot 2H_2O$ were purchased from Aladdin company, China and used without further purification. Throughout the experiment, distilled water was provided by a Water Purifier Nanopure system.

## 2. Characterization

The structure of CN, CN/x$NiMoP_2$ were investigated by power X-ray diffraction (XRD) measurement on a Rigaku SmartLab X-ray diffractometer. The morphology of the catalysts was measured by field emission scanning electron microscopy (XL 30 ESEM-FEG) and transmission electron microscopy (TEM, JEM-2010F). A Nicolet AVATAR 360 FT-IR spectrophotometer was operated to achieve the Fourier transform infrared (FT-IR) spectrum. The UV-Vis diffuse reflectance spectra (DRS) were obtained by a UV-Vis spectrophotometer of Shimadzu 3600 UV-Vis-NIR spectrophotometer (Cary 7000). Nitrogen adsorption-desorption isotherms and BET test were performed by using ASAP 2020M. The fluorescence spectra (PL) and time-resolved photoluminescence (TRPL) decay spectra were obtained by Edinburgh FLS920P. The X-ray photoelectron spectra (XPS) were conducted on a VG ESCALAB MKII spectrometer, employing Mg K excitation (1253.6 eV). Electron paramagnetic resonance (EPR) experiments were conducted at room temperature on an ER-200D spectrometer (Bruker, Germany). Thermogravimetric analysis (TGA) measurements were conducted using NETZSCH STA499F3 (air flow) with mass spectroscopy (MS, QMS403D).

**3. Electrochemical test analysis**

The photocurrent density and electrochemical impedance spectra (EIS) were acquired on a CHI 660E system (Shanghai Chenhua Instrument Co., Ltd, Shanghai, China) in a three-electrode system. The FTO/catalysts were used as the working electrode, a saturated Ag/AgCl electrode was used as the reference electrode, and a Pt sheet was used as the counter electrode. The working electrodes were prepared as follows: Typically, 35 mg of photocatalyst powder, 100 mg ethyl cellulose and 2 mL ethanol were mixed in an agate mortar and thoroughly ground for 60 min. Then, 0.5 mL of the solution was homogeneously spread on a FTO (1 cm×3 cm) glass substrate. After coating, the FTO glasses were calcined at 350 ºC for 2 h under air atmosphere. 0.5 M $Na_2SO_4$ was used as electrolyte at normal temperature, the light source was a 300 W Xe lamp with a UV cutoff filter (420 nm).

**4. Apparent quantum efficiency (AQE) calculations**

The measurement of apparent quantum efficiency (AQE) was carried out under the Xe lamp (300 W) equipped with different band-pass filters (420 nm). The intensity of irradiated light was recorded from a spectroradiometer (CEL-FZ-A, China).

The apparent quantum efficiency (AQE) was calculated by the Equation 1:

$$\mathrm{AQE}(\%) = \frac{2 \times \text{number of evolved H2 molecules}}{\text{number of incident photons}} \times 100\% \qquad (1)$$

$$= \frac{2n\mathrm{NAhc}}{PS\lambda t} \times 100\%$$

where $n$ is the evolution amount of $H_2$, $N_A$ is Avogadro's constant, h is Planck's constant, c is the speed of light, $\lambda$ is the wavelength of the incident light, $P$ is the power density, $S$ is the light exposure area, and $t$ is the reaction time.

Table S1. Calculated apparent quantum efficiency (AQE) at different wavelengths.

| Wavelength | $H_2$ Evolved (μmol) | Light Intensity | AQE |
|---|---|---|---|
| λ = 380 nm | 4.82 | 6.07 mW | 17.7% |
| λ = 400 nm | 4.29 | 8.17 mW | 11.1% |
| λ = 420 nm | 2.61 | 13.51 mW | 3.9% |
| λ = 450 nm | 1.55 | 9.77 mW | 3.0% |
| λ = 500 nm | 0.20 | 9.83 mW | 0.35% |

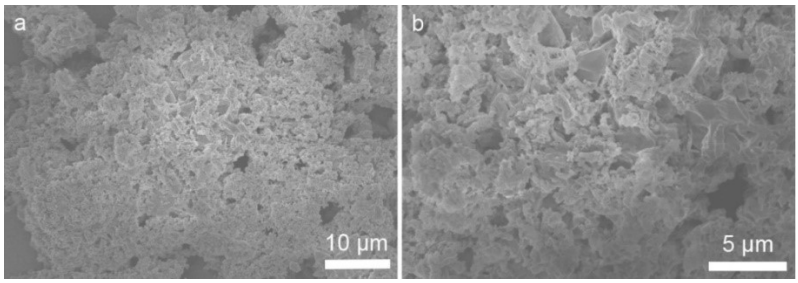


**Fig. S1** SEM images of CN.

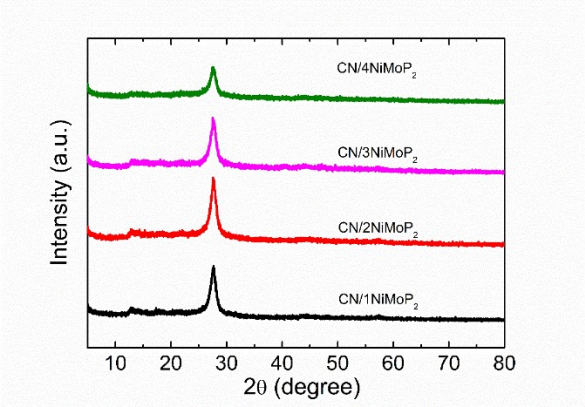


**Fig. S2** XRD patterns of CN/x$NiMoP_2$.

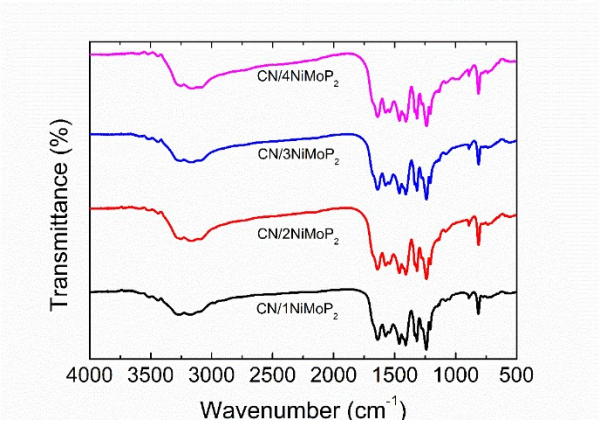


**Fig. S3** FTIR spectra of CN/xNiMoP$_2$.

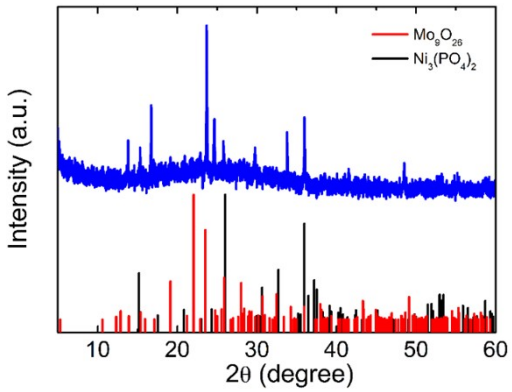


**Fig. S4** XRD pattern of the residue of CN/3NiMoP$_2$ composite after TGA measurement.

According to the **Fig. 3c** and **Fig. S4**,

$$m_{(Mo9O26)} + m_{(Ni3(PO4)2)} = 24.6\% * m_{(CN/3NiMoP2)} \quad (2)$$

$$n * M_{(Mo9O26)} + 3n * M_{(Ni3(PO4)2)} = 24.6\% * m_{(CN/3NiMoP2)} \quad (3)$$

here, m is the mass of sample. M is the relative molecular mass of sample. n is the amount of substance of $Mo_9O_{26}$. Since the elements Ni and Mo have the same amount of substance, the amount of substance of $Ni_3(PO_4)_2$ is 3n.

For $NiMoP_2$, the amount of substance is 9n. Therefore, the loading mass percentage of $NiMoP_2$ in CN/3NiMoP$_2$ was obtained by the following equation.

$$\omega\% = 9n * M_{(NiMoP2)} / m_{(CN/3NiMoP2)} * 100\% \quad (4)$$

Accordingly, $NiMoP_2$ in CN/3NiMoP$_2$ is about 19.5%.

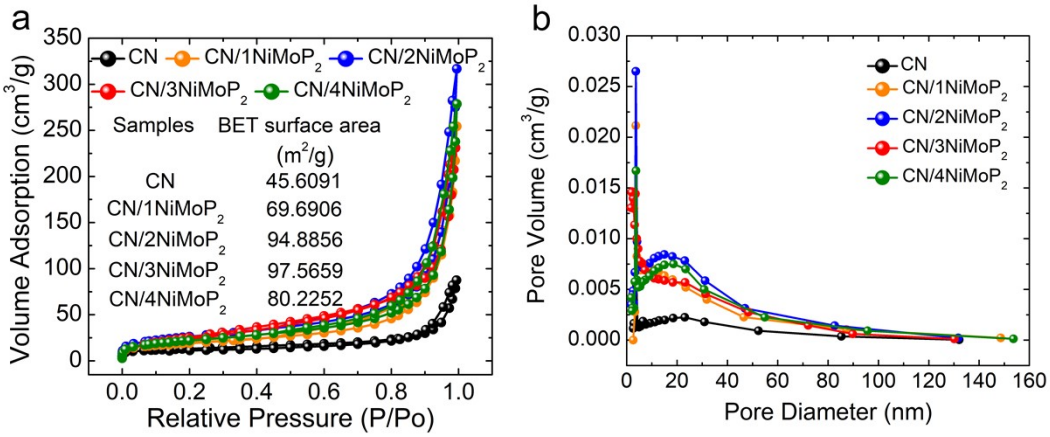


**Fig. S5** (a) Nitrogen adsorption-desorption; (b) Pore size distribution profiles of CN and CN/xNiMoP$_2$.

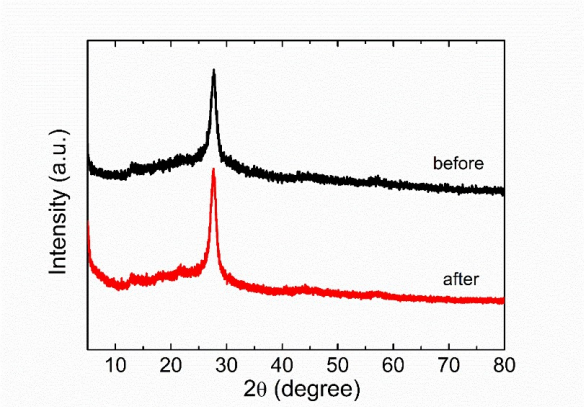


**Fig. S6** XRD of CN/3NiMoP$_2$ before and after cycling tests for $H_2$ production.

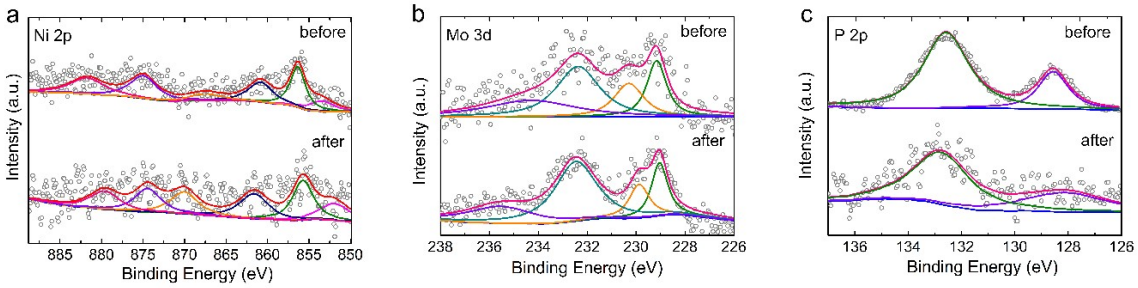


**Fig. S7** XPS of CN/3NiMoP$_2$ before and after cycling tests for $H_2$ production.

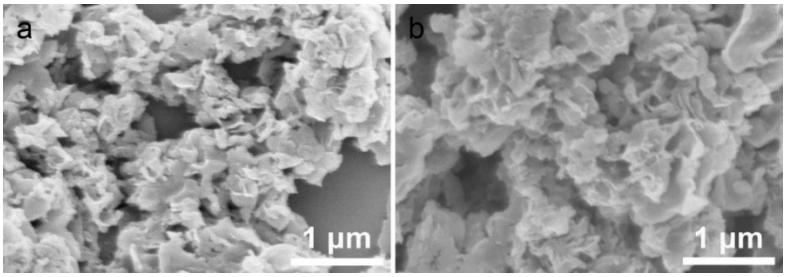


**Fig. S8** SEM of CN/3NiMoP$_2$ before and after cycling tests for $H_2$ production.

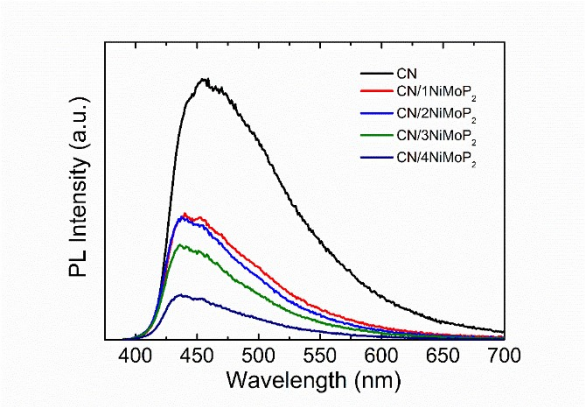


**Fig. S9** PL spectra of CN/xNiMoP$_2$.

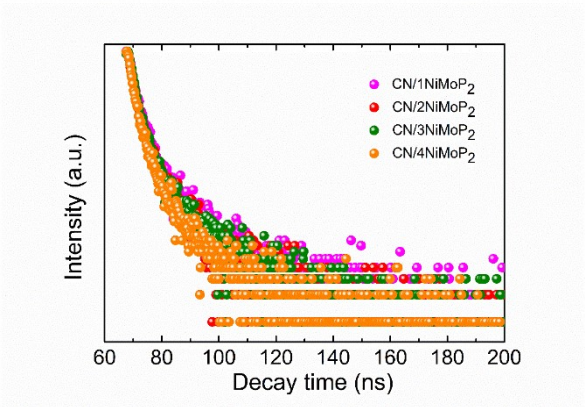


**Fig. S10** Time-resolved transient PL decay spectra of CN/xNiMoP$_2$.

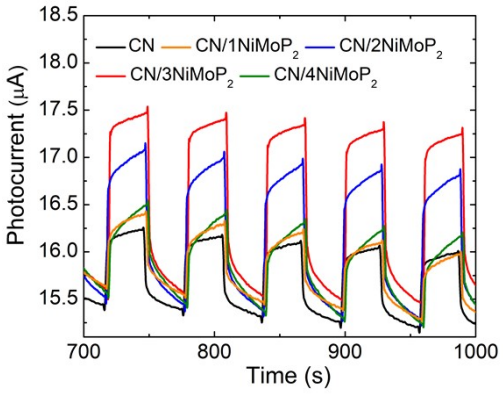


**Fig. S11** Transient photocurrent responses (i–t curves) of CN/xNiMoP$_2$ under visible-light irradiation (>420 nm).

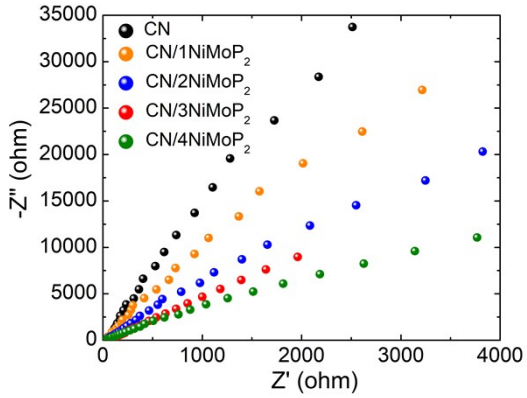


**Fig. S12** EIS spectra in the dark of CN/xNiMoP$_2$.

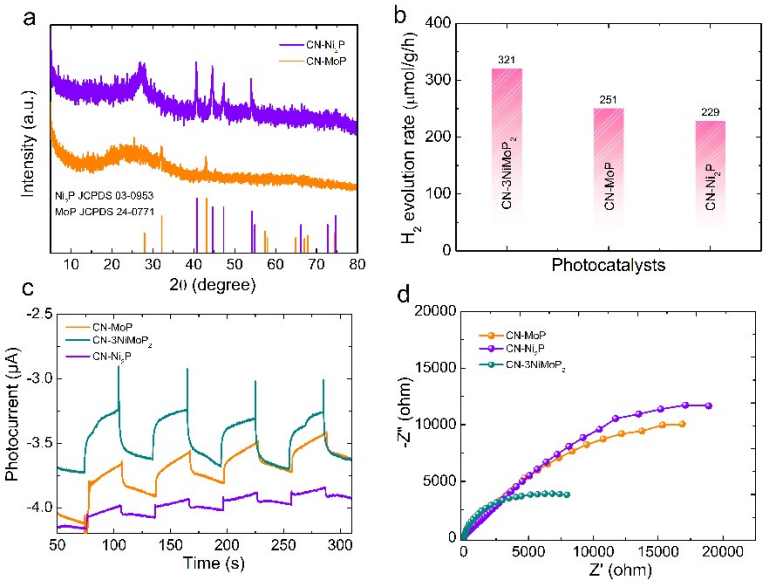


**Fig. S13** (a) XRD patterns of CN-Ni$_2$P and CN-MoP. (b) Photocatalytic H$_2$ production

rates of different samples (λ > 420 nm). (c) Transient photocurrent responses (i–t curves) under visible-light irradiation (>420 nm). (d) EIS spectra in the dark.

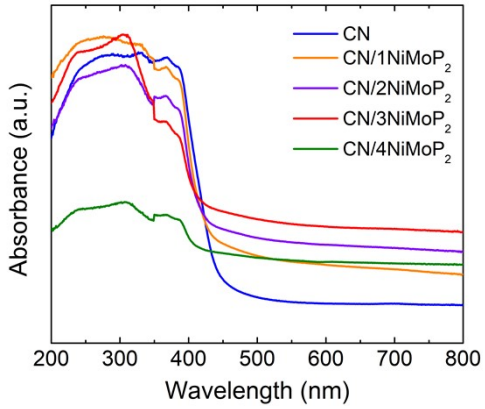


**Fig. S14** UV–vis diffuse reflectance spectra of CN/xNiMoP$_2$.

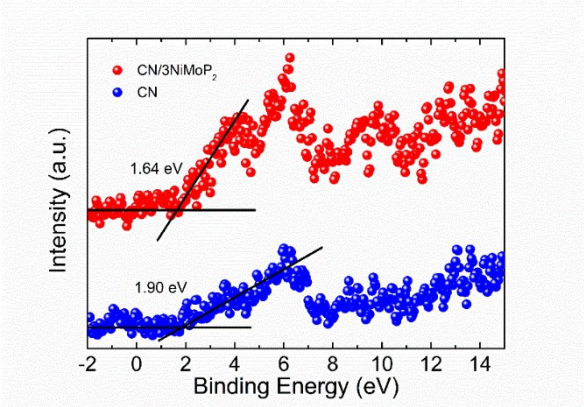


**Fig. S15** XPS valance band spectra of CN and CN/3NiMoP$_2$.

**Table S2.** The comparison of photocatalytic performance with cocatalysts in this work with other CN based ones for photocatalytic $H_2$ evolution in recent literatures.

| Photocatalyst | Cocatalyst | Light source | Reactant solution | Activity (μmol $h^{-1}$ $g^{-1}$) | AQE (%) | Ref. |
|---|---|---|---|---|---|---|
| **CN** | **$NiMoP_2$** | **300 W Xe lamp (λ>420nm)** | **TEOA** | **783** | **3.9 (420 nm)** | **This work** |
| CN | PA-Ni | visible light (λ > 420 nm) | MeOH | 713 | 2.8 (940 nm) | 1 |
| mpg-CN | $FeMoS_x$ | 300 W Xe lamp (λ>420nm) | TEOA | 551.42 | 4.0 (420 nm) | 2 |
| CN | $Co_3O_4$ | visible light | TEOA | 50 | None | 3 |
| CN | $Cu(OH)_2$ | visible light | TEOA | 187 | None | 4 |
| CN | $CoO_x$ | 300 W Xe lamp (λ>420nm) | TEA | 725.7 | 1.9 (420 nm) | 5 |
| CN | NCDS/$MoS_2$ | 300 W Xe lamp (λ > 420 nm) | TEOA | 212.41 | None | 6 |
| CN | $Ni(OH)_2$ | 300 W Xe lamp (λ > 400 nm) | TEOA | 87.2 | 8.2 (400 nm) | 7 |
| CN | Mo-$Mo_2C$ | 300 W Xe lamp (λ>420nm) | TEOA | 219.7 | 8.3 (420 nm) | 8 |
| CN | $Ni_2P$/NiO | 300 W Xe lamp (λ>420nm) | TEOA | 504 | 0.22 (400nm) | 9 |
| CN | FeP | 300 W Xe lamp (λ>420nm) | TEOA | 177.9 | 1.57 (420 nm) | 10 |

**References**


1. Y. Huang, Y. Jian, L. Li, D. Li, Z. Fang, W. Dong, Y. Lu, B. Luo, R. Chen, Y. Yang, M. Chen and W. Shi, *Angew. Chem. Int. Ed.*, 2021, **60**, 5245.
2. B. Wang, C. Yan, G. Xu, X. Shu, J. Lv and Y. Wu, *Chem. Eng. J.*, 2022, **427**, 131507.
3. L. Yang, J. Liu, L. Yang, M. Zhang, H. Zhu, F. Wang and J. Yin, *Renew. Energy,* 2020, **145**, 691.
4. S. Mahzoon, M. Haghighi and S. M. Nowee, *Renew. Energy*, 2020, **150**, 91-100.
5. Y. X. Zhu, T. Wan, X. M. Wen, D. W. Chu and Y. J. Jiang, *Appl. Catal. B: Environ.*, 2019, **244**, 814.
6. Y. Jiao, Q. Huang, J. Wang, Z. He and Z. Li, *Appl. Catal. B: Environ.*, 2019, **247**, 124.
7. R. Cao, H. Yang, S. Zhang and X. Xu, *Appl. Catal. B: Environ.*, 2019, **258**, 117997.
8. J. Dong, Y. Shi, C. P. Huang, Q. Wu, T. Zeng and W. F. Yao, *Appl. Catal. B: Environ.*, 2019, **243**, 27.
9. J.-W. Shi, Y. Zou, L. Cheng, D. Ma, D. Sun, S. Mao, L. Sun, C. He and Z. Wang, *Chem. Eng. J.*, 2019, **378**, 122161.
10. D. Zeng, T. Zhou, W.-J. Ong, M. Wu, X. Duan, W. Xu, Y. Chen, Y.-A. Zhu and D.-L. Peng, *ACS Appl. Mater. Interfaces*, 2019, **11**, 5651.